



Tidal Disruption Events from Stripped Stars

Brenna Mockler¹, Monica Gallegos-Garcia^{2,3}, Ylva Götberg^{1,4}, Jon M. Miller⁵, and Enrico Ramirez-Ruiz⁶

¹The Observatories of the Carnegie Institution for Science, Pasadena, CA 91101, USA; bmockler@carnegiescience.edu

²Department of Physics & Astronomy, Northwestern University, Evanston, IL 60208, USA

³Center for Interdisciplinary Exploration & Research in Astrophysics (CIERA), Northwestern University, Evanston, IL 60208, USA

⁴Institute of Science and Technology Austria, 3400 Klosterneuburg, Austria

⁵Department of Astronomy, University of Michigan, 1085 South University Avenue, Ann Arbor, MI 48109, USA

⁶Department of Astronomy and Astrophysics, University of California, Santa Cruz, CA 95064, USA

Received 2024 June 5; revised 2024 August 4; accepted 2024 August 6; published 2024 September 12

Abstract

Observations of tidal disruption events (TDEs) show signs of nitrogen enrichment reminiscent of other astrophysical sources such as active galactic nuclei and star-forming galaxies. Given that TDEs probe the gas from a single star, it is possible to test whether the observed enrichment is consistent with expectations from the CNO cycle by looking at the observed nitrogen/carbon (N/C) abundance ratios. Given that $\approx 20\%$ of solar-mass stars (and an even larger fraction of more massive stars) live in close binaries, it is worthwhile to also consider what TDEs from stars influenced by binary evolution would look like. We show here that TDEs from stars stripped of their hydrogen-rich (and nitrogen-poor) envelopes through previous binary-induced mass loss can produce much higher observable N/C enhancements than even TDEs from massive stars. Additionally, we predict that the time dependence of the N/C abundance ratio in the mass fallback rate of stripped stars will follow the inverse behavior of main-sequence stars, enabling a more accurate characterization of the disrupted star.

Unified Astronomy Thesaurus concepts: Supermassive black holes (1663); Tidal disruption (1696); Galaxy nuclei (609); Active galactic nuclei (16); Close binary stars (254); Broad-absorption line quasar (183); Carbon-nitrogen cycle (194); Ultraviolet transient sources (1854); X-ray transient sources (1852); Transient sources (1851); High energy astrophysics (739); Binary stars (154)

1. Introduction

With recent observations and new, more sensitive instruments, nitrogen enrichment has been appearing in a wide variety of astrophysical research: from quasars and active galactic nucleus (AGN) disks (e.g., Bentz et al. 2004) to distant star-forming galaxies (e.g., Bunker et al. 2023). Nitrogen enrichment is typically closely linked to the CNO cycle—the nuclear reaction that fuses hydrogen to helium in the deep interiors of massive stars. How nitrogen-enriched material is then exposed from its origin in the interior of massive stars remains a largely unsolved problem. This emphasizes the importance of understanding links between stellar evolution and a range of different astrophysical research fields and in a variety of different environments.

Recent observations of tidal disruption events (TDEs) show surprisingly high N/C abundance ratios (e.g., abundance ratios relative to solar of $N/C > 10$ in ASASSN-14li, iPTF15af, iPTF16fnl; see Cenko et al. 2016; Kochanek 2016a; Blagorodnova et al. 2017; Yang et al. 2017; Blagorodnova et al. 2019).⁷ These TDEs occur when stars are ripped apart by the supermassive black holes (SMBHs) in the centers of galaxies, after which the gas from the star is eventually accreted by the

SMBH, producing bright transient flares in the process (e.g., Rees 1988; Evans & Kochanek 1989; Guillochon & Ramirez-Ruiz 2013). High N/C abundance ratios suggest that the disrupted star was subject to the CNO cycle and therefore relatively massive, thus constituting a promising channel for enriching gas surrounding the SMBH. This was first proposed by Kochanek (2016a) and further investigated in Kochanek (2016b), Yang et al. (2017), and Mockler et al. (2022). With the increasing sample of TDEs now reaching $\gtrsim 100$ (e.g., Hammerstein et al. 2023), and with upcoming data from the Vera Rubin Observatory predicted to increase this number to $\gtrsim 1000$ (e.g., Bricman & Gomboc 2020), we can expect a wealth of TDE data soon to help improve our understanding of not only SMBHs but also stellar populations in the centers of galaxies.

Tidal disruptions of stars around SMBHs probe stellar populations on size scales that cannot be observed directly outside our own Galactic neighborhood. The stars that are disrupted originate from near the sphere of influence of the black hole, corresponding to size scales of order $\approx 0.5\text{--}10$ pc for SMBHs with masses between $\approx 10^5$ and $10^8 M_\odot$.

The increasing number of TDE observations has motivated the development of numerous light-curve and spectral models to attempt to explain the unique features of these events and also to use observations to constrain properties of the black hole and the disrupted star (Roth & Kasen 2018; Mockler et al. 2019; Ryu et al. 2020a; Wen et al. 2020; Metzger 2022) and better understand black hole accretion (Ramirez-Ruiz & Rosswog 2009; Dai et al. 2018; Andalman et al. 2022).

Much like in observations of AGN (e.g., Bentz et al. 2004; Jiang et al. 2008), measurements of spectral lines in TDEs hold the potential to constrain the composition of the irradiated gas in galactic nuclei. Unlike in AGN, in TDEs the gas producing

⁷ In addition to these three events, there are also a few newer TDEs with potential detections of broad UV nitrogen and/or carbon lines that might be used to constrain N/C ratios with further analysis. These include ASASSN-14ko (Payne et al. 2023), AT2018zr (Hung et al. 2019), AT2019qiz (Hung et al. 2021), and AT2020vdq (Somalwar et al. 2023).

the lines is predominantly from a single star, and so composition constraints in TDE spectra tell us about the properties of individual stars in the spheres of influence of the host galaxies. In some cases there may be a closer connection between these two phenomena—for example, Kochanek (2016a) proposed that the nitrogen enrichment seen in the broad-line region (BLR) of AGN (nitrogen-rich quasars) could sometimes originate from prior tidal disruptions, especially in galaxies with high rates of these transients (such as post-starburst galaxies; e.g., Arcavi et al. 2014; Law-Smith et al. 2019; French et al. 2020).

The observations of TDEs with unexpectedly high nitrogen abundances have complicated the previous assumption that most TDEs originated from low-mass main-sequence (MS) stars (which are generically nitrogen-poor), as is predicted if disrupted stars are drawn randomly from the stellar population given standard stellar initial mass functions. Mockler et al. (2022) showed that massive stars ($M > 2 M_{\odot}$) that fuse hydrogen through the CNO cycle are somewhat more consistent with these observations, since the abundance of nitrogen rises at the expense of carbon and oxygen in regions that experience the CNO cycle. However, recent reanalysis of X-ray data from the TDE ASASSN-14li by Miller et al. (2023) finds nitrogen/carbon abundances that push the limits of what is expected even from the disruption of massive stars. Main-sequence stars have nitrogen-rich cores, but their envelopes are nitrogen-poor. During a TDE, dilution by in-mixing of the nitrogen-poor envelope should make the abundance ratio less pronounced.

Motivated by these results, in this work we explore what the disruption of a star stripped of its hydrogen-rich (and therefore nitrogen-poor) envelope would look like and how it would compare to the disruption of stars at various stages of stellar evolution. Such “stripped stars” are expected to be created through binary interaction over the full stellar mass range, but we explore stripped stars originating from massive stellar evolution, as they will result in higher N/C abundance ratios. Throughout this work, we will use N/C to mean the abundance ratio of nitrogen to carbon relative to the solar value.⁸

2. The Compositional Structure of Stripped Stars

Stripped stars have naturally nitrogen-enriched and carbon-depleted outer layers (Götberg et al. 2018). This originates from the previous MS evolution when hydrogen fused to helium through the CNO cycle. The slowest reaction in the CNO cycle is proton capture onto nitrogen, which causes a buildup of nitrogen at the expense of carbon and oxygen in regions that have experienced or are experiencing the CNO cycle (e.g., Burbidge et al. 1957). As the convective MS core recedes in mass coordinate, seen from outside and inward, it leaves a layer that is gradually enriched in helium but that also has nitrogen enrichment from the CNO cycle throughout it. During envelope stripping in binaries, the thick hydrogen-rich (and nitrogen-poor) *envelope* is removed, revealing the chemically enriched layer. Because of this, the surfaces of stripped stars contain a small amount of hydrogen (notably still sufficient to produce strong hydrogen lines in supernovae; Dessart et al. 2011, 2012), contain a large amount of helium,

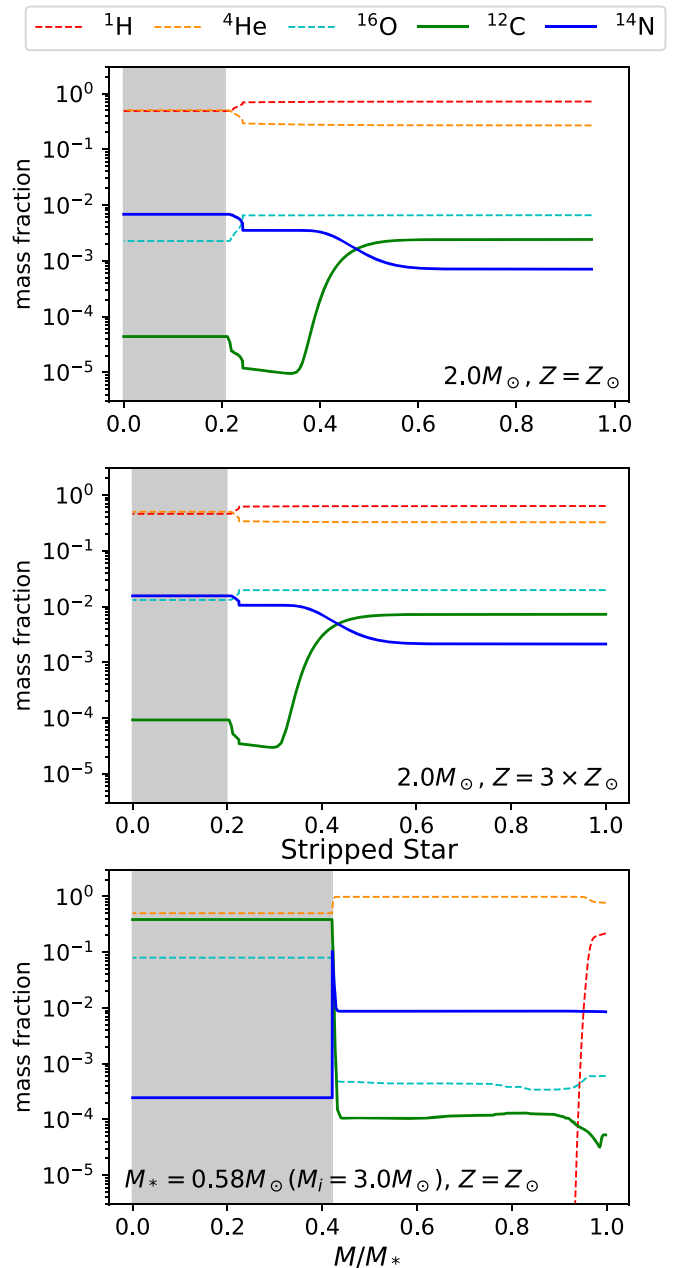


Figure 1. Composition as a function of mass fraction for three representative stars. The top panel shows a $2 M_{\odot}$ MS star born at Z_{\odot} , the middle panel shows a $2 M_{\odot}$ MS star born at $3 Z_{\odot}$, and the bottom panels shows a stripped star born at Z_{\odot} with an initial mass of $3 M_{\odot}$ and a current mass of $0.58 M_{\odot}$. All three stars have $Y_{\text{C}} = 0.5$. The two MS stars are halfway through hydrogen burning, and the stripped star is halfway through helium burning. The gray shaded regions denote the convectively burning core (including convection and convective overshoot).

and are enriched in nitrogen (Hirsch 2009; Heber 2016; Götberg et al. 2023; see also Drilling et al. 2013).

After envelope stripping is complete, the stripped star starts fusing helium to carbon and oxygen in the center (Laplace et al. 2021). The central region is convective, but it is relatively small, and there is also a substantial radiative layer that previously was the MS core and now extends to the stellar surface. The described composition structure is depicted in Figure 1, where we show a model for a $0.58 M_{\odot}$ stripped star (with initial mass $M_i = 3 M_{\odot}$; bottom panel) compared with models for $2 M_{\odot}$ MS stars born at two different metallicities

⁸ Note that the mass abundance ratio relative to solar is equivalent to the number abundance ratio relative to solar, as the ratio of the mass of the elements cancels out.

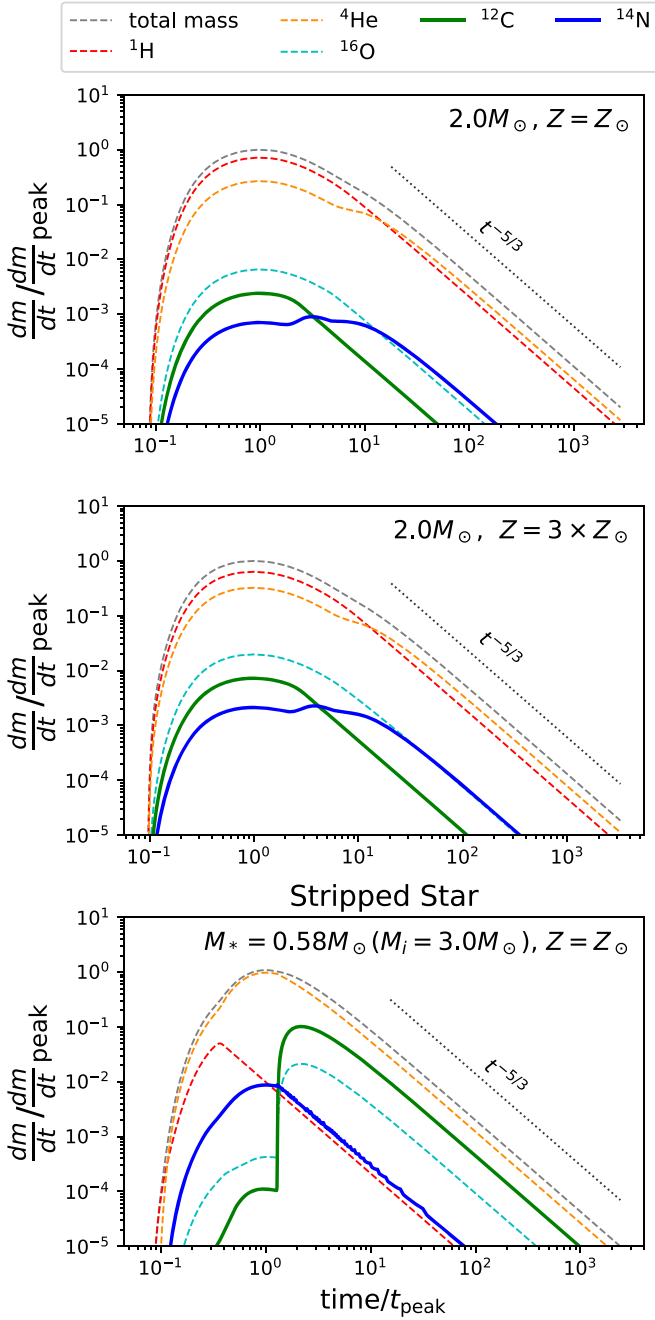


Figure 2. We plot analytical fallback rates calculated for various MESA stellar models. Fallback rates for different elements are plotted separately in addition to the overall fallback rate. All fallback rates are scaled by the peak fallback rate and peak timescale for all material (see Figure 4 for a comparison with hydro simulations in physical units). The top two panels feature our fiducial $2 M_{\odot}$ single stars near the end of their MS lifetime at $Y_c = 0.9$. The bottom panel features our $0.58 M_{\odot}$ stripped star halfway through He core burning at $Y_c = 0.5$.

that are undergoing CNO cycle hydrogen burning (top, middle). In this study, we consider the gray shaded (convective) regions the core and the white (radiative) regions the envelope. The MS stars are born at solar metallicity (Z_{\odot} ; top panel) and $3 \times$ solar metallicity ($3 Z_{\odot}$; middle panel). In Figure 1, all three models are plotted when the mass fraction of

helium at the center of the star $Y_c = 0.5$. The MS models are halfway through hydrogen burning, and the stripped star is halfway through helium burning.⁹ All models were computed with the MESA stellar evolution code (Paxton et al. 2011, 2013, 2015, 2018, 2019; Jermyn et al. 2023), and the stripped star model was published in Götberg et al. (2018, see their Table 1). We have chosen these masses for analysis because they are on the lower end of the mass range that experience CNO burning and are therefore representative of the most common stars with nitrogen enhancements from CNO burning.¹⁰ We will continue to use these same three stellar models throughout the Letter (at various stages of their evolution).

To summarize, the entirety of stripped stars are made up of material that has previously experienced CNO burning; however, their convective cores are currently undergoing helium burning. Because of this, their N/C abundance ratios are high in their radiative outer regions (leftover from their MS core CNO burning) but low in their convective cores, where helium burning is ongoing. This is in contrast to MS stars sufficiently massive to experience CNO burning, whose nitrogen-rich cores are embedded within nitrogen-poor outer layers. Therefore, to first order, the abundances in the center versus the outer layers of stripped stars exhibit the opposite trends compared to solar-type MS stars (see Figure 1). As we will show, this means that the time-dependent composition evolution in the material returning to an SMBH after the tidal disruption of stripped stars should follow the inverse behavior of CNO-burning MS stars.

3. Connections to Observations

We begin with a very brief overview of the tidal disruption process and go on to describe how the disruption of a stripped star differs from (and is similar to) that of a MS star.

Tidal disruption occurs when the binding energy of a star is overwhelmed by the tidal gravity of a black hole. The radius of disruption for a star of mass M_* and radius R_* by a black hole of mass M_h can be approximated by setting the self-gravity of the star equal to the tidal force of the black hole, which gives the canonical tidal radius $R_t = R_* \left(\frac{M_*}{M_h} \right)^{1/3}$. The “depth” of disruption relative to R_t can be described using the impact parameter $\beta = R_t/R_p$, where deeper (smaller pericenter radius, R_p) disruptions have larger values of β . The rate of return of gas to an SMBH after a star is tidally disrupted depends on the binding energy distribution in the gas (e.g., Lodato et al. 2009; Guillochon & Ramirez-Ruiz 2013; Law-Smith et al. 2020; Ryu et al. 2020b). In a full disruption, where the core is destroyed, material in the outer layers of the star (which is more bound to the black hole) will return first, and material from the core of the star (which is less bound to the black hole) will return later. Once the slope of the binding energy distribution as a function of stellar mass becomes relatively constant (as we approach the core of the star), the mass fallback rate approaches the

⁹ This is equivalent to $0.47 \times$ and $0.4 \times$ the terminal-age MS (TAMS) lifetimes, respectively, for the Z_{\odot} and $3 Z_{\odot}$ MS models and to $0.5 \times$ the stripped star’s helium-burning lifetime for that model.

¹⁰ We chose this $3 M_{\odot}$ model for the stripped star because the structure was numerically robust at smaller scales. The qualitative features are the same for a stripped star with a $2 M_{\odot}$ progenitor.

canonical value of $t^{-5/3}$:

$$\frac{dm}{dt} = \frac{dm}{de} \times \frac{de}{dt} \quad (1)$$

$$\frac{dm}{dt} = \frac{dm}{de} \times \frac{(2\pi GM_h)^{2/3}}{3} t^{-5/3}. \quad (2)$$

Here $\frac{dm}{dt}$ is the mass return rate to the black hole, $\frac{dm}{de}$ is the mass–energy distribution in the debris, and $\frac{de}{dt}$ is the derivative of the orbital energy with respect to orbital timescale and orbital energy, which can be calculated analytically from Kepler’s laws.

3.1. Composition Evolution

If the star’s composition varies with radius (and therefore also with binding energy), this radial stratification transforms into a time dependence, where the composition of the gas returning to the black hole varies with time. This has been explored for MS stars analytically in Gallegos-Garcia et al. (2018) and with hydrodynamical simulations in Law-Smith et al. (2019).

A key result in both is that the ratio of N/C in the fallback material varies dramatically with time and is dependent on the mass and age of the star. As discussed in Section 2, the composition profile of a stripped star is, to first order, the inverse of the profile of a MS star (see also Figure 1). In Figure 2, we plot the normalized, time-dependent composition of the fallback rate for our two MS stars and compare it to the composition of the fallback rate of our stripped star (of similar progenitor mass). We calculate the fallback rates analytically using the frozen-in approximation described in Lodato et al. (2009) and Kesden (2012) and apply this framework to MESA stellar models as outlined in Gallegos-Garcia et al. (2018).

While we know that the analytical fallback rates do not exactly match the peak magnitude and timescales of fallback rates from hydrodynamic simulations (and for this reason we scale out these quantities from our composition plots), they should capture overall trends in the composition as a function of time.¹¹ Hydrodynamic simulations of solar-mass MS stars have shown a similar transition in the abundances of nitrogen, carbon, and oxygen (and the abundance ratio of N/C) in the fallback material of a TDE compared to analytical calculations. This transition corresponds to when material from the core begins to return to the SMBH. Simulations do find that this transition occurs more gradually than analytical treatments predict and that it begins slightly before peak instead of slightly after peak (Law-Smith et al. 2019). Because of this, we expect mixing in the hydrodynamics of disruption to also smear out the sharp transition we see in the relative abundance of these elements in the stripped star (these complications are discussed in more detail in Section 3.3).

We find that the mass fractions of nitrogen and carbon vary much more dramatically in the disruption from our stripped star compared to the MS stars throughout the fallback evolution (see Figure 2). This is despite comparing to MS stars near the end of their MS lifetimes with $Y_c = 0.9$.¹² Naively, we might expect the material returning at late times in a MS star

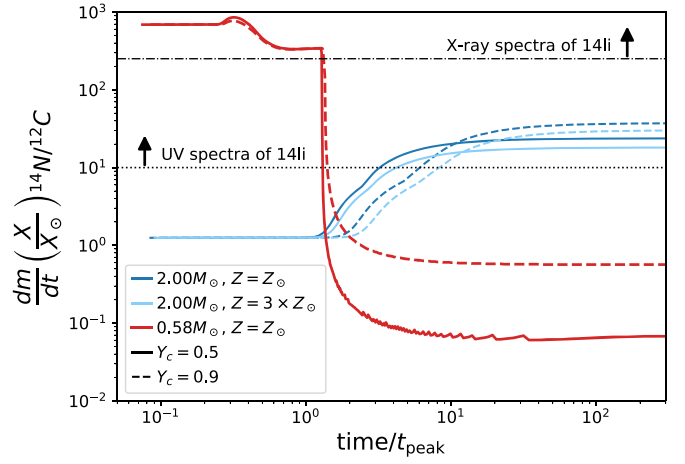


Figure 3. The analytical N/C abundance ratio (relative to solar) in the mass fallback rate as a function of time since disruption (scaled by t_{peak} , which we expect to be of order \sim week timescales; see Figure 4). We plot our $0.58 M_{\odot}$ stripped star ($M_i = 3 M_{\odot}$) at the beginning of helium core burning ($Y_c = 0.9$; red solid line) and halfway through helium core burning ($Y_c = 0.5$; red dashed line). We plot our $2 M_{\odot}$ MS stars partway through the MS and nearing the end of the MS. The Z_{\odot} MS model is plotted in dark blue, and the $3 \times Z_{\odot}$ MS model is plotted in light blue ($Y_c = 0.5$ plotted as solid lines; $Y_c = 0.9$ plotted as dashed lines). Constraints from UV and X-ray spectra from the transient ASASSN-14li are plotted as dotted and dashed–dotted lines, respectively.

disruption (and therefore including material from the core) to be similar to the material that returns at early times for the stripped star (given that the envelope of the stripped star is made up of material that was near the core when it was on the MS). However, because tidal disruption is an inherently aspherical process, we are not probing purely radial slices at each point in time. Instead we are probing vertical slices (compared to the orbital plane of the black hole and star), and so while material that returns at later times does have more material from the core, it is mixed with material from the outer layers as well (see Figure 1 in Gallegos-Garcia et al. 2018 for reference). On the other hand, material that returns at early times originates almost completely from the envelope of the star. This means that for a MS star material from the core that returns at late times and is enhanced in N/C will be diluted by material from the outer layers, whereas for a stripped star material that returns at early times from the envelope and is also enhanced in N/C will not be as diluted and will retain a higher N/C abundance.

We also find that there is comparatively little difference between the relative mass fractions and N/C abundance ratios in the fallback rates of a MS star born at solar metallicity and one born at $3 \times$ solar metallicity (top two panels of Figure 2, light-blue and dark-blue lines in Figure 3). The curves for elements other than hydrogen are shifted up for the higher-metallicity star compared to the solar-metallicity star (as expected), but the relative abundances are very similar. The N/C abundance ratio is actually slightly higher at late times in the solar-metallicity model than in the higher-metallicity model. This is because the core of the solar-metallicity model makes up a slightly larger fraction of the total mass (the N/C ratio in the core is not significantly larger; it is simply slightly less diluted by the outer layers of the star).

In Figure 3, we focus on just the N/C abundance in the fallback material and compare this time-dependent composition ratio for stellar models at different stages of evolution. We plot the stripped star and the MS stars at $Y_c = 0.5$ and $Y_c = 0.9$. For

¹¹ See Section 3.2 and Figure 4 for a comparison with fallback curves from simulations.

¹² This is equivalent to 0.94 and $0.96 \times$ TAMS for the Z_{\odot} and $3 \times Z_{\odot}$ stars, respectively.

the MS stars, this is partway through the MS ($Y_c = 0.5$) and near the end of the MS ($Y_c = 0.9$). For the stripped star, this is early on in helium burning ($Y_c = 0.9$) and halfway through helium burning ($Y_c = 0.5$).¹³

Notably, we find that the composition of the fallback rate from the stripped star TDE can naturally explain the very high N/C ratios observed in the X-ray spectra of ASASSN-14li (dashed-dotted lines in Figure 3). While moderately massive ($M_* \gtrsim 1\text{--}2 M_\odot$) MS stars provide a good explanation for the high N/C constraints measured in the UV (Yang et al. 2017; Mockler et al. 2022), the much higher constraints from X-ray measurements are better matched by the stripped star’s fallback rate (Miller et al. 2023). We discuss ASASSN-14li as a potential stripped star TDE candidate further in Section 3.4.

3.2. Fallback Rate

The fallback rate of gas to an SMBH after disruption has been well studied, and predictions from hydrodynamic simulations have largely converged (e.g., Ramirez-Ruiz & Rosswog 2009; Guillochon & Ramirez-Ruiz 2013; Cheng & Bogdanović 2014; Tejeda et al. 2017; Gafton & Rosswog 2019; Law-Smith et al. 2020; Ryu et al. 2020b). However, previous work focuses on the disruptions of noninteracting stars that evolved through single stellar evolution, and most previous work also focuses on MS stars.¹⁴

Stripped stars are more compact (have smaller radii) than MS stars; however, we find that their scaled density profiles are actually well approximated by $2 M_\odot$ MS stars. Relatedly, their central density divided by their average density ($\rho_c/\bar{\rho}$)—a proxy for the disruptability of a star (Law-Smith et al. 2020; Ryu et al. 2020a)—is also similar to the value for MS stars. This is convenient, as the density profile and central concentration of a star determine both the critical impact parameter for full disruption (the minimum impact parameter for full disruption, above which all disruptions are full disruptions; Guillochon & Ramirez-Ruiz 2013; Law-Smith et al. 2020; Ryu et al. 2020a; Coughlin & Nixon 2022) and the shape of the resulting mass fallback rate to the black hole.

In Figure 4, we compare the density profiles of our stripped stellar models (taken from Götzberg et al. 2018) with the density profiles of various MS stars, as well as a $\gamma = 4/3$ polytropic model. We see that the density profile of a $2 M_\odot$ MS star with $Y_c = 0.5$ is a very good approximation of our fiducial stripped star model (also with $Y_c = 0.5$). From looking at the evolution between the $Y_c = 0.5$ and $Y_c = 0.9$ models for the MS star and stripped star, respectively, it is also clear that the structure of the stripped star changes less dramatically over its helium-burning lifetime as the structure of the MS star changes over its hydrogen-burning lifetime. We also compare the central density over the average density ($\rho_c/\bar{\rho}$) for the $2 M_\odot$ star and the stripped star over their full evolution (MS for the $2 M_\odot$ star, MS and helium core burning for the stripped star). The values for $\rho_c/\bar{\rho}$ during helium core burning for the stripped star are similar to the values for the MS star during the middle third of its MS evolution. Using the analytical formula for the impact parameter as a function of $\rho_c/\bar{\rho}$ from Law-Smith et al. (2020)

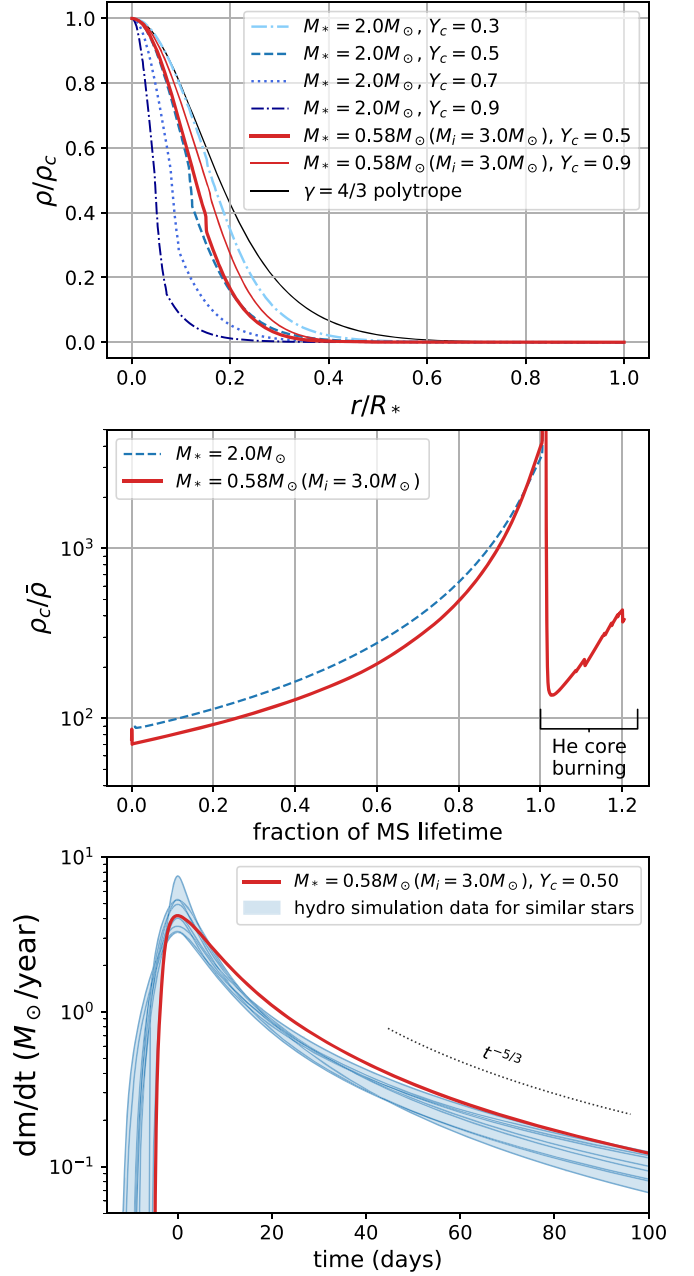


Figure 4. Top: comparison of the density profile of a stripped star ($M_* = 0.58 M_\odot$, $M_i = 3 M_\odot$) with the density profiles of a $2 M_\odot$ star at various stages of stellar evolution. A polytropic stellar profile ($\gamma = 4/3$) is also plotted for comparison. We scale the density profile by the central density (ρ_c) and scale the radii by the stellar radius (R_*). Middle: the central density (ρ_c) divided by the average density ($\bar{\rho} = M_*/(4/3\pi R_*^3)$) for the same stellar models. For the stripped star, we plot $\rho_c/\bar{\rho}$ for both the MS (pre-stripping) and the He core burning sequence (post-stripping). Bottom: mass fallback rates from various hydrodynamical simulations (blue; from Law-Smith et al. 2020) compared to the analytical fallback rate calculated for the stripped star (red). The hydro fallback rates are from full disruptions of stars with similar density profiles and central concentrations to the stripped star, scaled to the mass and radius of the stripped star (and to $M_h = 10^{6.8} M_\odot$, a reasonable estimate for ASASSN-14li).

($\beta_{\text{crit}} \approx 0.5(\rho_c/\bar{\rho})^{1/3}$), we find that this corresponds to critical impact parameters for full disruption between $2.5 < \beta_{\text{crit}} < 3.5$.

Using the information from the top two panels of Figure 4, in the bottom panel we have plotted a range of hydrodynamical fallback rates from Law-Smith et al. (2020) for stars with

¹³ This is equivalent to 0.5 and 0.12 of the way through the stripped star’s helium-burning lifetime.

¹⁴ Notable exceptions are papers on red giant disruptions (e.g., MacLeod et al. 2012; Bogdanović et al. 2014) and white dwarf disruptions (e.g., Rosswog et al. 2009; Haas et al. 2012; Law-Smith et al. 2017; Kawana et al. 2018).

similar stellar structures to our stripped star.¹⁵ To compare with our analytical fallback rate, we scale these hydrodynamical fallback rates by the mass and radius of the stripped star using the canonical $t_{\text{peak}} \propto M_*^{-1} R_*^{3/2}$ and $\dot{M}_{\text{peak}} \propto M_*^2 R_*^{-3/2}$ relations. Given that we have specifically chosen stars with similar density profiles and values of $\rho_c/\bar{\rho}$, this should give peak timescales and fallback rates consistent with the updated equations for these parameters presented in Coughlin & Nixon (2022) and Bandopadhyay et al. (2023) (which reduce to the canonical relations when holding $\rho_c/\bar{\rho}$ constant).

3.3. Outflows

Observations of TDEs provide estimates for the size scales of gas around the black hole from the disrupted star through measurements of blackbody photosphere radii and wind radii and velocities (e.g., Alexander et al. 2016; Hung et al. 2017; Kara et al. 2018; Mockler et al. 2019; Wevers et al. 2024). Additionally, broad, blueshifted lines have been observed in many TDEs, consistent with lines forming in dense, outflowing gas (e.g., Arcavi et al. 2014; Holoien et al. 2016; Roth & Kasen 2018; Nicholl et al. 2020). Lines are expected to form somewhere between the photosphere and outer wind radius and therefore should be dependent on the composition of the photosphere and outflows.

We predict that outflows from TDEs of stripped stars will have a nitrogen-enhanced outer layer, with N/C abundance ratios up to $50 \times$ higher than is achievable with MS stars (see Figure 3). Emission lines produced by the irradiated outflow would therefore show strong N/C enhancements at early times. Then, as the wind expands and material that returned to the black hole at later times is illuminated, the relative strength of N/C would flip, and carbon would be enhanced relative to nitrogen. The exact timing of this behavior and the amount of gas with very high N/C abundance ratios depend on how much mixing occurs. If the gas in the outermost layers of the star that is most bound to the black hole is mixed with material deeper in the star either in the disruption process or in the circularization and accretion processes that launch the outflows, then the N/C abundance will be lower and will decrease more rapidly.

While hydro simulations are necessary to truly determine the extent of the mixing, we provide some limits here. If the material in the outer layer of the star experiences minimal mixing during the disruption process and outflows are launched promptly after material first returns to the black hole, then it is possible that all material launched in outflows during the rise of the light curve is highly nitrogen enriched. While there is debate on the length of time between when material begins to return to the black hole and when a flare is produced, most previous results agree that once a bright flare is produced outflows should also be launched. This could be through shocks and stream collisions, through disk winds, or through both processes (e.g., Dai et al. 2018; Bonnerot et al. 2021; Steinberg & Stone 2024; Huang et al. 2023; Price et al. 2024).

In Figure 5, we plot the range of radii for a wind launched between model estimates of when material began to return to the black hole and when the light curve peaked for the transient ASASSN-14li, and we compare to observations (this event is

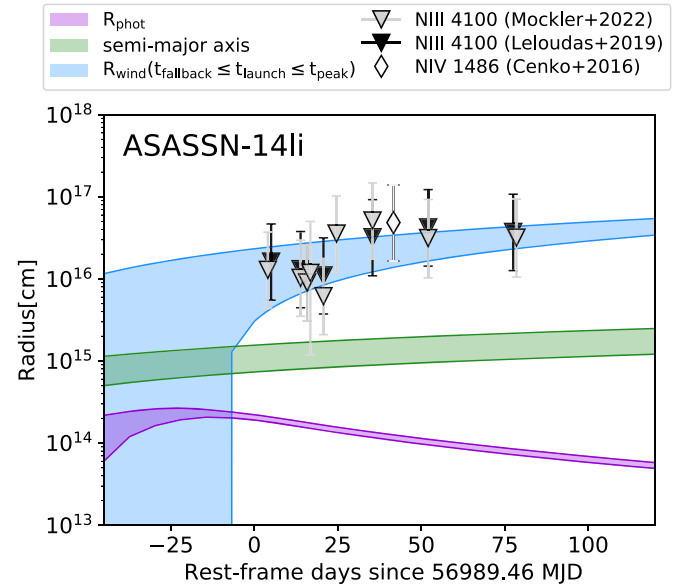


Figure 5. Radii of gas in TDE ASASSN-14li, originally estimated in Mockler et al. (2022) using the `MOSFIT` transient fitting code. The x-axis is time in rest-frame days since the first observation. We have plotted in blue the radii outflows would reach if launched between first fallback and peak of the mass fallback rate (assuming a velocity of $0.1c$, based on radio observations of the event). This corresponds to the time range in the mass fallback rate during which our analytical model predicts a large N/C enhancement. We overplot the virial radii of various nitrogen lines observed in the event, including a UV measurement (white diamond) that puts constraints on the N/C ratio of the debris. We also plot the radii of the blackbody photosphere and semimajor axis of returning debris in purple and green, respectively.

discussed in more detail in the following section). We assume that there is minimal delay between when material returns to the black hole and when luminosity and outflows are produced. If there is a longer delay, material will be N/C enhanced for less time/over a smaller radius range. Regardless, if N/C enhancement is observed from the disruption of a stripped star, the N/C abundance ratio of material surrounding the black hole should decrease with time.

3.4. Comparing to ASASSN-14li

Nitrogen lines are measured in optical spectra of ASASSN-14li from MJD 56993 to 57129 (Cenko et al. 2016; Holoien et al. 2016; Brown et al. 2018); however, the more constraining UV and X-ray detections of high nitrogen/carbon abundance ratios occurred between MJD 56999 and 57002 (XMM and Chandra X-ray spectra; Miller 2015; Miller et al. 2023) and on MJD 57032 (Hubble Space Telescope (HST) UV spectra; Cenko et al. 2016). The X-ray spectra constrain the N/C abundance ratio to be ≥ 300 relative to the Sun in material close to the black hole near the peak of the light curve, and the UV spectra constrain the N/C ratio to be ≥ 10 in material at much larger radii on the decline of the light curve. Interestingly, the N/C ratio in the envelope of the stripped stars we analyze is also ≥ 300 (see Figure 3). As we show in this section, the measurements from both X-ray and UV observations are consistent with coming from material that returned to the black hole before the peak of the fallback rate and was then subsequently fed to the accretion disk or ejected in outflows.

As discussed in the previous section, if the flare was from the disruption of a stripped star, material that returns to the black hole at early times and up to the peak of the fallback rate

¹⁵ We included full disruptions of all stars with $36 < \rho_c/\bar{\rho} < 756$ from Law-Smith et al. (2020). These include a TAMS $0.7 M_{\odot}$ star, zero-age MS (ZAMS)-TAMS $1 M_{\odot}$ star, ZAMS $1.5 M_{\odot}$, and ZAMS $3 M_{\odot}$ star.

(which we are assuming here to be approximately coincident with the peak of the optical and UV light curve, as is predicted by many models; e.g., Mockler et al. 2019; Ryu et al. 2020a; Steinberg & Stone 2024) is likely to be heavily enhanced in nitrogen with respect to carbon (see Figure 3). Unfortunately, the peak of the transient ASASSN-14li was not observed; however, radio observations place rough estimates on the time that outflows were first launched to be between MJD ~ 56884 and 56990 (Alexander et al. 2016), and light-curve analysis places estimates on the peak of the light curve to be between MJD ~ 56944 and 56990 (e.g., Mockler et al. 2019). Given this information, the early outflows launched before MJD ~ 56990 and material accreted around the same time would likely have high N/C abundance ratios if the material came from a stripped star.

There is much theoretical debate on the nature of the initial luminosity production during the rise of TDEs; however, multiple theoretical models have shown that it is reasonable for material to start to circularize into a disk by the time of the fallback rate and light curve’s peak (e.g., Bonnerot et al. 2021; Andalman et al. 2022; Steinberg & Stone 2024). The observations of X-ray spectra in Miller et al. (2023) were taken starting on MJD 56999. The X-rays are therefore consistent with being emitted from a disk made up of material that mostly fell back before peak but only recently circularized (and would be nitrogen enriched if from a stripped star), combined with additional material that has fallen back after peak. While it is expected that the X-ray emission originates from close to the black hole in the forming disk, the UV emission is consistent with originating from optically thick outflows at larger radii. These outflows would come from gas that returned to the black hole at earlier times and was then ejected through, e.g., stream collisions or disk winds (Dai et al. 2018; Bonnerot et al. 2021).

In Figure 5 we show that the virial velocities measured from the widths of nitrogen lines in the optical and UV spectra are consistent with the range of radii where gas from outflows launched before peak would be at the time of the observations. We plot an estimate of the gas geometry surrounding ASASSN-14li based on light-curve fits and the wind velocity measured in radio observations (adapted from Mockler et al. 2022). If the material is not virialized and gas broadening dominates the line widths instead (Roth & Kasen 2018; Parkinson et al. 2022), the gas could also originate at smaller radii, where it would be more likely to be mixed with material from the core of the star that returns at later times. For a stripped star, this would mean material that is not enhanced in N/C (see, e.g., Figure 3). The UV spectra constrain the N/C abundance ratio to be $\geq 10 \times$ solar metallicity—a limit that is much lower than the N/C ratio in the envelope of a stripped star (N/C ≥ 300). Therefore, even if the lines originate at smaller radii from a mix of gas from the outer layers and the core, this could still be consistent with the disruption of a stripped star.

4. Discussion

Here we discuss additional relevant points that can be investigated further in the future.

Partial and Repeated TDEs: If a stripped star is partially disrupted instead of fully disrupted, the core will remain intact and the material that is bound to the black hole will come entirely from the envelope. In this case, all of the material that

returns to the black hole will have high N/C abundance ratios (both before and after peak). Partial disruptions are likely intrinsically more common than full disruptions, as two-body relaxation processes produce significantly more partial disruptions than full disruptions (e.g., Stone & Metzger 2016). However, they are expected to be more difficult to observe. First of all, less accreted material likely means less luminous events. Additionally, if optical and UV emission is due to reprocessing, then less accreted material also means that optical and UV emission will make up a smaller fraction of the total emitted luminosity (e.g., Roth et al. 2016). Given this, we expect partial TDEs from stripped stars to produce lower-luminosity, X-ray-bright TDEs with consistently high N/C ratios.

In the case of *repeated* partial disruptions (“repeated TDEs”), the flares should eventually switch from nitrogen-rich to nitrogen-poor as subsequent disruptions remove material from deeper within the star. Interestingly, repeated TDEs from stripped stars are theoretically predicted to survive longer and therefore potentially produce more flares than repeated TDEs from MS stars. This is because the core fraction is larger in stripped stars than most MS stars, which results in the star contracting instead of expanding when a small amount of mass is removed (Liu et al. 2023). It is possible a stripped star could explain the repeated partial disruption ASASSN-14ko (Payne 2021), as this event has survived for years without significant evolution observed in its flares (as would be expected if its core mass fraction was $\lesssim 0.3$; Liu et al. 2023). This event actually might be nitrogen-poor at later times given the appearance of strong C III lines in the UV without obvious N III counterparts in the HST spectra taken during flares 18 and 19 (Payne et al. 2023; unfortunately, there are no UV spectra from earlier flares to compare with). However, this event also appears to require a star of at least $\sim 2 M_{\odot}$ to explain the observed luminosity with reasonable mass-to-energy efficiencies (e.g., $\epsilon \sim 0.01$, consistent with predictions of inefficient accretion for these events; Liu et al. 2023), and so a stripped star from a larger mass progenitor ($\gtrsim 7 M_{\odot}$) would be required (Götberg et al. 2018).

Rates of Stripped Star TDEs: A detailed rate calculation is outside the scope of this Letter, but a brief overview of how the number of stripped stars compares to the total stellar population is still useful. An important caveat is that here we only discuss binary-stripped stars—stars in galactic nuclei may also be stripped through other avenues such as stellar collisions (e.g., Rose et al. 2023; Gibson et al. 2024, submitted to ApJ) or partial tidal disruptions (e.g., Bortolas 2022; Liu et al. 2023).

The fraction of roughly solar-mass, solar-metallicity stars born in close binaries is ≈ 0.2 (Badenes et al. 2018; Moe et al. 2019). This fraction increases with stellar mass and with metallicity (e.g., it is ≈ 0.4 for stars above $4 M_{\odot}$; Moe & Di Stefano 2017; Badenes et al. 2018; Lee et al. 2020; Jadhav et al. 2021). It also increases toward the centers of clusters owing to mass segregation (e.g., Mathieu & Latham 1986; Geller & Mathieu 2012; Milone et al. 2012). We will conservatively assume that half of these close binaries will merge before producing a stripped star (e.g., Clausen et al. 2012), and so one in four stars in close binaries will eventually be stripped by their companion. Therefore, we will assume that 5% of low-mass stars and 10% of higher-mass stars ($\gtrsim 4 M_{\odot}$) will eventually be stripped. Envelope stripping is completed after the MS, meaning that stripped stars can be quite long-

lived, as the helium core burning stage remains. For massive stars, the stripped star stage corresponds to about 10% of the total stellar lifetime. However, for stars with initial masses $\lesssim 4 M_\odot$, the lack of a thick hydrogen-burning shell stops the helium core from substantial growth, and these stars can therefore live much longer as stripped—up to half of the total stellar lifetime (e.g., Götberg et al. 2018; Arancibia-Rojas et al. 2024). Given this, we might expect at least $\sim 1\%$ – 2.5% of stars in galactic nuclei that have experienced the CNO cycle to be stripped stars ($0.2 \times 0.25 \times 0.5 = 0.025$ for the smallest stars, $0.4 \times 0.25 \times 0.1 = 0.01$ for larger stars).

The smaller radii and greater compactness of stripped stars make them more difficult to partially disrupt than MS stars; however, their critical disruption radii for core disruption are less than a factor of 10 different¹⁶ than the critical radii for MS stars (as might be expected given their similar values of $\rho_c/\bar{\rho}$). Given that the TDE rate from two-body relaxation scales as $\propto R_t^{1/4}$ for a wide range of tidal radii and black hole masses (e.g., Wang & Merritt 2004; Milosavljević et al. 2006; MacLeod et al. 2012), the likelihood of full disruption for stars after being stripped and during their helium-burning sequence is, at any given time, within a factor of two ($\lesssim 10^{1/4} = 1.8$) of the likelihood of full disruption for the same stars during their MS. Therefore, we might expect at least $\sim 0.6\%$ – 1.4% of the disruptions of stars *born* at $M_* \gtrsim 1 M_\odot$ to come from stripped stars (including other factors such as the age, metallicity, and mass segregation of stellar populations should increase this percentage). We can organize this estimate as follows:

$$f_{\text{TDE,stripped}} \approx f_{\text{close binary}} \times \frac{1}{4} \times \frac{\tau_{\text{stripped}}}{\tau_*} \times \left(\frac{R_{t,\text{stripped}}}{R_{t,\text{MS}}} \right)^{1/4}. \quad (3)$$

Here $f_{\text{close binary}}$ is the fraction of stars born in close binaries— $f_{\text{close binary}} \sim 0.2$ (0.4) for low-mass (higher-mass) stars. The factor of $\frac{1}{4}$ represents the probability that the close binary results in a stripped star (we assume that $\approx 1/2$ of binaries merge; e.g., Clausen et al. 2012), multiplied by the probability that it is the stripped star, and not its companion, that is disrupted by the black hole (another factor of $1/2$). Then, τ_{stripped} and τ_* are the stripped star and total stellar (MS + stripped) lifetimes— $\frac{\tau_{\text{stripped}}}{\tau_*} \sim 0.5$ (0.1) for low-mass (higher-mass) stars. And finally, $R_{t,\text{stripped}}$ and $R_{t,\text{MS}}$ are the critical tidal radii for core disruption for stripped stars and MS stars, respectively— $\frac{R_{t,\text{stripped}}}{R_{t,\text{MS}}} \gtrsim 0.1$ for the majority of binary-stripped stars (using stripped star parameters from Götberg et al. 2018 throughout). This leads to $f_{\text{TDE,stripped}} \sim 0.014$ (0.0055) for low-mass (high mass) stars, or $\sim 0.6\%$ – 1.4% of TDEs from stars born at masses such that they will undergo CNO burning ($M_* \gtrsim 1 M_\odot$). We note that although it would seem that the fraction of higher-mass stripped stars is small, Wolf–Rayet stars (massive, helium-burning stars that have lost much of their hydrogen envelopes) are observed in our own Galactic center (e.g., Lu et al. 2013).

The smaller tidal radii of stripped stars compared to MS stars also mean that the maximum black hole mass that can disrupt a stripped star is smaller than the maximum black hole mass that can disrupt a MS star (by a factor of $(R_{t,\text{stripped}}/R_{t,\text{MS}})^{3/2}$). This means that for a population of TDEs from stripped stars, the median mass of the disrupting black hole should be smaller and the direct capture drop-off (observed for the general population of TDEs; e.g., van Velzen et al. 2020; Yao et al. 2023) should be lower. If $R_{t,\text{stripped}}/R_{t,\text{MS}} \sim 5$ (as it is for our fiducial model), this would mean that the drop-off for stripped stars would occur at a black hole mass that is a factor of ~ 10 lower—between $\sim 10^{6.5}$ and $10^{7.5} M_\odot$ instead of between $\sim 10^{7.5}$ and $10^{8.5} M_\odot$ as calculated for MS stars.

Connections to Nitrogen Enrichment in AGN Disks:

Regions associated with galactic centers have been found to be nitrogen enriched, for example, through the spectra of AGN BLRs (e.g., Bentz et al. 2004; Batra & Baldwin 2014). TDE searches have, up to this point, mostly excluded AGN host galaxies, and so a preexisting nitrogen-rich BLR is disfavored to explain nitrogen-rich TDEs. However, it is still possible that AGN and TDEs share the same source of nitrogen enrichment.

The centers of galaxies also often have higher-than-solar overall metallicities. Some studies have found that all BLR line measurements in those galaxies (not just N/C ratios) are consistent with supersolar metallicities (e.g., Batra & Baldwin 2014), and therefore nitrogen enhancements can be explained by these higher overall metallicities. Others find that the enhancement of nitrogen is higher than that of other metals (Jiang et al. 2008; Matsuoka et al. 2017) and therefore cannot be explained solely by increasing the overall metallicity of the galactic nuclei. The most common explanation put forward for general metallicity enhancement is high star formation rates in the vicinity of the SMBH (consistent with observations of star formation gradients in galaxies (e.g., Nelson et al. 2016), but at size scales not easily testable observationally). To explain anomalously high nitrogen abundances with respect to the overall metallicity, Matsuoka et al. (2017) invoke mass loss from AGB winds enriching the BLR gas with nitrogen (which was dredged up from CNO-processed material near the core). This scenario also requires in situ star formation to create sufficient AGB stars. Additionally, it predicts higher AGN accretion rates, as some of the winds will end up accreted by the SMBH (Davies et al. 2007). It does appear that nitrogen-loud quasars have higher Eddington ratios than the general population, in line with the prediction of AGB winds enriching BLR clouds and also increasing SMBH accretion rates (Matsuoka et al. 2017).

High star formation rates in the centers of galaxies would also help explain the nitrogen enhancement found in some TDEs, as it would increase the fraction of higher-mass stars undergoing CNO cycle burning. However, high star formation rates alone are likely not sufficient to explain the unexpectedly high rate of nitrogen-enhanced TDEs (Mockler et al. 2022). Additionally, higher overall metallicities in the centers of galaxies are not sufficient to explain the particularly extreme nitrogen enhancement found in ASASSN-14li (see Figures 2 and 3), unless these high birth metallicities are accompanied by unusually high N/C abundance ratios, or young stars are polluted by winds from massive stars. These two scenarios have been suggested to explain highly nitrogen-enhanced stars in globular clusters (although these globular cluster stars are still less nitrogen enhanced than ASASSN-14li appears to be;

¹⁶ For example, the critical disruption radius for our fiducial stripped star is within a factor of 5–6 of the critical disruption radius for the $2 M_\odot$ MS star we compare it to. See Section 3.2 for a more in-depth discussion of how the critical disruption radius is determined.

Larsen et al. 2014; Bastian & Lardo 2018). On the other hand, TDEs can clearly contribute to the nitrogen enhancement of an SMBH’s environment, and it is possible that this contribution is important to the population of nitrogen-enhanced AGN. This connection is particularly intriguing if the galaxy is in a post-starburst phase of evolution, or if the nuclear cluster hosts an SMBH binary given that these environments (1) appear conducive to AGN activity (e.g., Dodd et al. 2021) and (2) produce TDE rates that are observed or predicted to be $\gtrsim 20\text{--}100 \times$ higher than average (e.g., French et al. 2016; Graur et al. 2018; Law-Smith et al. 2019; French et al. 2020; Hammerstein et al. 2021; Melchor et al. 2023; Mockler et al. 2023).

5. Summary of Key Points

Here we briefly summarize the main takeaways from this work:






1. TDEs probe stellar populations in galactic nuclei, and recent observations of N/C abundances in TDEs point to the disruption of stars born at moderately high masses that show chemical enrichment indicative of the CNO cycle.
2. X-ray spectral observations of ASASSN-14li show N/C abundance lower limits that are so high ($\gtrsim 300$) that they are difficult to explain with MS evolution alone (Miller et al. 2023). In a MS star, the core has high N/C ratios, but the envelope is more carbon than nitrogen. In a TDE, when material from the core eventually falls back to the black hole, it is diluted by the carbon in the envelope material that falls back with it, limiting the maximum N/C abundance in fallback material (see Figure 3).
3. Binary-stripped stars have the reverse compositional structure of MS stars. Their helium-rich envelopes have high N/C abundance ratios, and it is their cores that are nitrogen poor and carbon enhanced (see Figure 1). When these stars are tidally disrupted, nitrogen-rich material from the envelope will return to the black hole first, without being diluted by nitrogen-poor material from the core. This means that the composition of fallback material from a tidally disrupted stripped star can have much higher enhancements of N/C than disruptions of MS stars.
4. Stripped stars also naturally produce the opposite N/C time evolution compared to MS stars and should therefore be observationally distinct in time series of their spectra (see Figure 3).

Acknowledgments

This work was performed in part at Aspen Center for Physics, which is supported by National Science Foundation grant PHY-2210452. We thank the participants and organizers of the summer Aspen 2023 workshop on “Stellar Interactions and the Transients They Cause” for fruitful discussions. B.M. is grateful for support from the Carnegie Theoretical Astrophysics Center. M.G.-G. is grateful for the support from Northwestern University’s Presidential Fellowship. E.R.-R. thanks the Heising-Simons Foundation, NSF (AST-2150255 and AST-2307710), Swift (80NSSC21K1409, 80NSSC19K1391), and Chandra (22-0142) for support.

Software: astropy (Astropy Collaboration et al. 2013).

ORCID iDs

Brenna Mockler  <https://orcid.org/0000-0001-6350-8168>
 Monica Gallegos-Garcia  <https://orcid.org/0000-0003-0648-2402>
 Ylva Göteborg  <https://orcid.org/0000-0002-6960-6911>
 Jon M. Miller  <https://orcid.org/0000-0003-2869-7682>
 Enrico Ramirez-Ruiz  <https://orcid.org/0000-0003-2558-3102>

References

- Alexander, K. D., Berger, E., Guillochon, J., Zauderer, B. A., & Williams, P. K. G. 2016, *ApJ*, 819, L25
- Andalman, Z. L., Liska, M. T. P., Tchekhovskoy, A., Coughlin, E. R., & Stone, N. 2022, *MNRAS*, 510, 1627
- Arancibia-Rojas, E., Zorotovic, M., Vučković, M., et al. 2024, *MNRAS*, 527, 11184
- Arcavi, I., Gal-Yam, A., Sullivan, M., et al. 2014, *ApJ*, 793, 38
- Astropy Collaboration, Robitaille, T. P., Tollerud, E. J., et al. 2013, *A&A*, 558, A33
- Badenes, C., Mazzola, C., Thompson, T. A., et al. 2018, *ApJ*, 854, 147
- Bandopadhyay, A., Fancher, J., Athian, A., et al. 2023, *ApJL*, 961, L2
- Bastian, N., & Lardo, C. 2018, *ARA&A*, 56, 83
- Batra, N. D., & Baldwin, J. A. 2014, *MNRAS*, 439, 771
- Bentz, M. C., Hall, P. B., & Osmer, P. S. 2004, *AJ*, 128, 561
- Blagorodnova, N., Cenko, S. B., Kulkarni, S. R., et al. 2019, *ApJ*, 873, 92
- Blagorodnova, N., Gezari, S., Hung, T., et al. 2017, *ApJ*, 844, 46
- Bogdanović, T., Cheng, R. M., & Amaro-Seoane, P. 2014, *ApJ*, 788, 99
- Bonnerot, C., Lu, W., & Hopkins, P. F. 2021, *MNRAS*, 504, 4885
- Bortolas, E. 2022, *MNRAS*, 511, 2885
- Bricman, K., & Gomboc, A. 2020, *ApJ*, 890, 73
- Brown, J. S., Kochanek, C. S., Holoiien, T. W. S., et al. 2018, *MNRAS*, 473, 1130
- Bunker, A. J., Saxena, A., Cameron, A. J., et al. 2023, *A&A*, 677, A88
- Burbidge, E. M., Burbidge, G. R., Fowler, W. A., & Hoyle, F. 1957, *RvMP*, 29, 547
- Cenko, S. B., Cucchiara, A., Roth, N., et al. 2016, *ApJ*, 818, L32
- Cheng, R. M., & Bogdanović, T. 2014, *PhRvD*, 90, 064020
- Clausen, D., Wade, R. A., Kopparapu, R. K., & O’Shaughnessy, R. 2012, *ApJ*, 746, 186
- Coughlin, E. R., & Nixon, C. J. 2022, *MNRAS*, 517, L26
- Dai, L., McKinney, J. C., Roth, N., Ramirez-Ruiz, E., & Miller, M. C. 2018, *ApJL*, 859, L20
- Davies, R. I., Müller Sánchez, F., Genzel, R., et al. 2007, *ApJ*, 671, 1388
- Dessart, L., Hillier, D. J., Li, C., & Woosley, S. 2012, *MNRAS*, 424, 2139
- Dessart, L., Hillier, D. J., Livne, E., et al. 2011, *MNRAS*, 414, 2985
- Dodd, S. A., Law-Smith, J. A. P., Auchettl, K., Ramirez-Ruiz, E., & Foley, R. J. 2021, *ApJ*, 907, L21
- Drilling, J. S., Jeffery, C. S., Heber, U., Moehler, S., & Napiwotzki, R. 2013, *A&A*, 551, A31
- Evans, C. R., & Kochanek, C. S. 1989, *ApJL*, 346, L13
- French, K. D., Arcavi, I., & Zabludoff, A. 2016, *ApJ*, 818, L21
- French, K. D., Wevers, T., Law-Smith, J., Graur, O., & Zabludoff, A. I. 2020, *SSRv*, 216, 32
- Gafton, E., & Rosswog, S. 2019, *MNRAS*, 487, 4790
- Gallegos-Garcia, M., Law-Smith, J., & Ramirez-Ruiz, E. 2018, *ApJ*, 857, 109
- Geller, A. M., & Mathieu, R. D. 2012, *AJ*, 144, 54
- Gibson, C. F., Kiroğlu, F., Lombardi, J. C., et al. 2024, *ApJ*, submitted
- Göteborg, Y., de Mink, S. E., Groh, J. H., et al. 2018, *A&A*, 615, A78
- Göteborg, Y., Drout, M. R., Ji, A. P., et al. 2023, *ApJ*, 959, 125
- Graur, O., French, K. D., Zahid, H. J., et al. 2018, *ApJ*, 853, 39
- Guillochon, J., & Ramirez-Ruiz, E. 2013, *ApJ*, 767, 25
- Haas, R., Shcherbakov, R. V., Bode, T., & Laguna, P. 2012, *ApJ*, 749, 117
- Hammerstein, E., Gezari, S., van Velzen, S., et al. 2021, *ApJ*, 908, L20
- Hammerstein, E., van Velzen, S., Gezari, S., et al. 2023, *ApJ*, 942, 9
- Heber, U. 2016, *PASP*, 128, 082001
- Hirsch, H. A. 2009, PhD thesis, Univ. of Erlangen-Nürnberg
- Holoiien, T. W. S., Kochanek, C. S., Prieto, J. L., et al. 2016, *MNRAS*, 455, 2918
- Huang, X., Davis, S. W., & Jiang, Y.-f. 2023, *ApJ*, 953, 19
- Hung, T., Cenko, S. B., Roth, N., et al. 2019, *ApJ*, 879, 119
- Hung, T., Gezari, S., Blagorodnova, N., et al. 2017, *ApJ*, 842, 29
- Hung, T., Foley, R. J., Veilleux, S., et al. 2021, *ApJ*, 917, 9
- Jadhav, V. V., Roy, K., Joshi, N., & Subramaniam, A. 2021, *AJ*, 162, 264

- Jermyn, A. S., Bauer, E. B., Schwab, J., et al. 2023, *ApJS*, 265, 15
- Jiang, L., Fan, X., & Vestergaard, M. 2008, *ApJ*, 679, 962
- Kara, E., Dai, L., Reynolds, C. S., & Kallman, T. 2018, *MNRAS*, 474, 3593
- Kawana, K., Tanikawa, A., & Yoshida, N. 2018, *MNRAS*, 477, 3449
- Kesden, M. 2012, *PhRvD*, 85, 24037
- Kochanek, C. S. 2016a, *MNRAS*, 458, 127
- Kochanek, C. S. 2016n, *MNRAS*, 461, 371
- Laplace, E., Justham, S., Renzo, M., et al. 2021, *A&A*, 656, A58
- Larsen, S. S., Brodie, J. P., Grundahl, F., & Strader, J. 2014, *ApJ*, 797, 15
- Law-Smith, J., Guillochon, J., & Ramirez-Ruiz, E. 2019, *ApJ*, 882, L25
- Law-Smith, J., MacLeod, M., Guillochon, J., Macias, P., & Ramirez-Ruiz, E. 2017, *ApJ*, 841, 132
- Law-Smith, J. A. P., Coulter, D. A., Guillochon, J., Mockler, B., & Ramirez-Ruiz, E. 2020, *ApJ*, 905, 141
- Lee, Y.-N., Offner, S. S. R., Hennebelle, P., et al. 2020, *SSRv*, 216, 70
- Liu, C., Mockler, B., Ramirez-Ruiz, E., et al. 2023a, *ApJ*, 944, 184
- Lodato, G., King, A. R., & Pringle, J. E. 2009, *MNRAS*, 392, 332
- Lu, J. R., Do, T., Ghez, A. M., et al. 2013, *ApJ*, 764, 155
- MacLeod, M., Guillochon, J., & Ramirez-Ruiz, E. 2012, *ApJ*, 757, 134
- Mathieu, R. D., & Latham, D. W. 1986, *AJ*, 92, 1364
- Matsuoka, K., Nagao, T., Maiolino, R., et al. 2017, *A&A*, 608, A90
- Melchor, D., Mockler, B., Naoz, S., Rose, S., & Ramirez-Ruiz, E. 2023, *ApJ*, 960, 14
- Metzger, B. D. 2022, *ApJ*, 937, L12
- Miller, J. M., Mockler, B., Ramirez-Ruiz, E., et al. 2023, *ApJ*, 953, L23
- Miller, M. C. 2015, *ApJ*, 805, 83
- Milone, A. P., Piotto, G., Bedin, L. R., et al. 2012, *A&A*, 540, A16
- Milosavljević, M., Merritt, D., & Ho, L. C. 2006, *ApJ*, 652, 120
- Mockler, B., Guillochon, J., & Ramirez-Ruiz, E. 2019, *ApJ*, 872, 151
- Mockler, B., Melchor, D., Naoz, S., & Ramirez-Ruiz, E. 2023, *ApJ*, 959, 18
- Mockler, B., Twum, A. A., Auchettl, K., et al. 2022, *ApJ*, 924, 70
- Moe, M., & Di Stefano, R. 2017, *ApJS*, 230, 15
- Moe, M., Kratter, K. M., & Badenes, C. 2019, *ApJ*, 875, 61
- Nelson, E. J., van Dokkum, P. G., Förster Schreiber, N. M., et al. 2016, *ApJ*, 828, 27
- Nicholl, M., Wevers, T., Oates, S. R., et al. 2020, *MNRAS*, 499, 482
- Parkinson, E. J., Knigge, C., Matthews, J. H., et al. 2022, *MNRAS*, 510, 5426
- Paxton, B., Bildsten, L., Dotter, A., et al. 2011, *ApJS*, 192, 3
- Paxton, B., Cantiello, M., Arras, P., et al. 2013, *ApJS*, 208, 4
- Paxton, B., Marchant, P., Schwab, J., et al. 2015, *ApJS*, 220, 15
- Paxton, B., Schwab, J., Bauer, E. B., et al. 2018, *ApJS*, 234, 34
- Paxton, B., Smolec, R., Schwab, J., et al. 2019, *ApJS*, 243, 10
- Payne, A. V., Shappee, B. J., Hinkle, J. T., et al. 2021, *ApJ*, 910, 125
- Payne, A. V., Auchettl, K., Shappee, B. J., et al. 2023, *ApJ*, 951, 134
- Price, D. J., Liptai, D., Mandel, I., et al. 2024, *ApJL*, 971, 17
- Ramirez-Ruiz, E., & Rosswog, S. 2009, *ApJL*, 697, L77
- Rees, M. J. 1988, *Natur*, 333, 523
- Rose, S. C., Naoz, S., Sari, R., & Linial, I. 2023, *ApJ*, 955, 30
- Rosswog, S., Ramirez-Ruiz, E., & Hix, W. R. 2009, *ApJ*, 695, 404
- Roth, N., & Kasen, D. 2018, *ApJ*, 855, 54
- Roth, N., Kasen, D., Guillochon, J., & Ramirez-Ruiz, E. 2016, *ApJ*, 827, 3
- Ryu, T., Krolik, J., & Piran, T. 2020a, *ApJ*, 904, 73
- Ryu, T., Krolik, J., Piran, T., & Noble, S. C. 2020b, *ApJ*, 904, 98
- Somalwar, J. J., Ravi, V., Yao, Y., et al. 2023, arXiv:2310.03782
- Steinberg, E., & Stone, N. C. 2024, *Natur*, 625, 463
- Stone, N. C., & Metzger, B. D. 2016, *MNRAS*, 455, 859
- Tejeda, E., Gafton, E., Rosswog, S., & Miller, J. C. 2017, *MNRAS*, 469, 4483
- van Velzen, S., Holoien, T. W. S., Onori, F., Hung, T., & Arcavi, I. 2020, *SSRv*, 216, 124
- Wang, J., & Merritt, D. 2004, *ApJ*, 600, 149
- Wen, S., Jonker, P. G., Stone, N. C., Zabludoff, A. I., & Psaltis, D. 2020, *ApJ*, 897, 80
- Wevers, T., Guolo, M., Pasham, D. R., et al. 2024, *ApJ*, 963, 17
- Yang, C., Wang, T., Ferland, G. J., et al. 2017, *ApJ*, 846, 150
- Yao, Y., Ravi, V., Gezari, S., et al. 2023, *ApJL*, 955, 31